

Table 6.11 Average data from cyclic polarisation scans - Freddie's Water flow conditions.

Alloy	Corrosion Potential (mV)	Pitting Potential (mV)	Passive Range (mV)	Perfectly Passive Range (mV)	Hysteresis Loop
1200	-697	-589	108	0	infinite
3004	-714	-537	177	70	large
5251	-743	-539	204	116	large
6063TB	-744	-459	285	0	infinite
6063TF	-695	-534	161	0	infinite
7017	-783	n/a	0	0	infinite
3CR12	-128	262	390	0	infinite
316L	-56	388	444	318	small
317L	-63	363	426	388	small
2205	-84	380	464	334	small

6.2.3 POTENTIODYNAMIC SCANS IN FREDDIE'S WATER - STATIC CONDITIONS.

This section only includes tests carried out at 40°C under static conditions in both aerated and de-aerated mine water. Temperature effects will be discussed later.

6.2.3.1 Aerated conditions

Alloy 1200 showed a passive region of around 90mV and a low corrosion rate of 12,3µm/year. All the other alloys with the exception of 7017 also showed regions of spontaneous passivation. Their general corrosion rates varied between a minimum of 12,1µm/year for alloy 3004 to 22,4µm/year for alloy 6063TF, with a massive 229,4µm/year for alloy 7017. The free corrosion potentials (E_{corr}) and the general corrosion rates obtained are summarised below in Table 6.12.

Table 6.12 Corrosion rates and E_{corr} values for static conditions in Freddie's mine water at 40°C.

Alloy	Average Corrosion Potential (mV)	Average Corrosion Rate (µm/year)
1200	-639	12,3
3004	-623	12,1
5251	-659	17,0
6063TB	-649	22,4
6063TF	-654	10,7
7017	-786	229,4
M.S.	-669	60,0
3CR12	-168	2,8
316L	-169	3,8

Even though 3CR12 appears to have a lower corrosion rate than 316L, it must be noted that values of this order are low accuracy and are indicative of the fact that the corrosion rate is insignificant.

6.2.3.1 Aerated conditions

Alloy 1200 showed a passive region of around 90mV and a low corrosion rate of 12,3µm/year. All the other alloys with the exception of 7017 also showed regions of spontaneous passivation. Their general corrosion rates varied between a minimum of 12,1µm/year for alloy 3004 to 22,4µm/year for alloy 6063TF, with a massive 229,4µm/year for alloy 7017. The free corrosion potentials (E_{corr}) and the general corrosion rates obtained are summarised below in Table 6.12.

Table 6.12 Corrosion rates and E_{corr} values for static conditions in Freddie's mine water at 40°C.

Alloy	Average Corrosion Potential (mV)	Average Corrosion Rate (µm/year)
1200	-639	12,3
3004	-623	12,1
5251	-659	17,0
6063TB	-649	22,4
6063TF	-654	10,7
7017	-786	229,4
M.S.	-669	60,0
3CR12	-168	2,8
316L	-169	3,8

Even though 3CR12 appears to have a lower corrosion rate than 316L, it must be noted that values of this order are low accuracy and are indicative of the fact that the corrosion rate is insignificant.

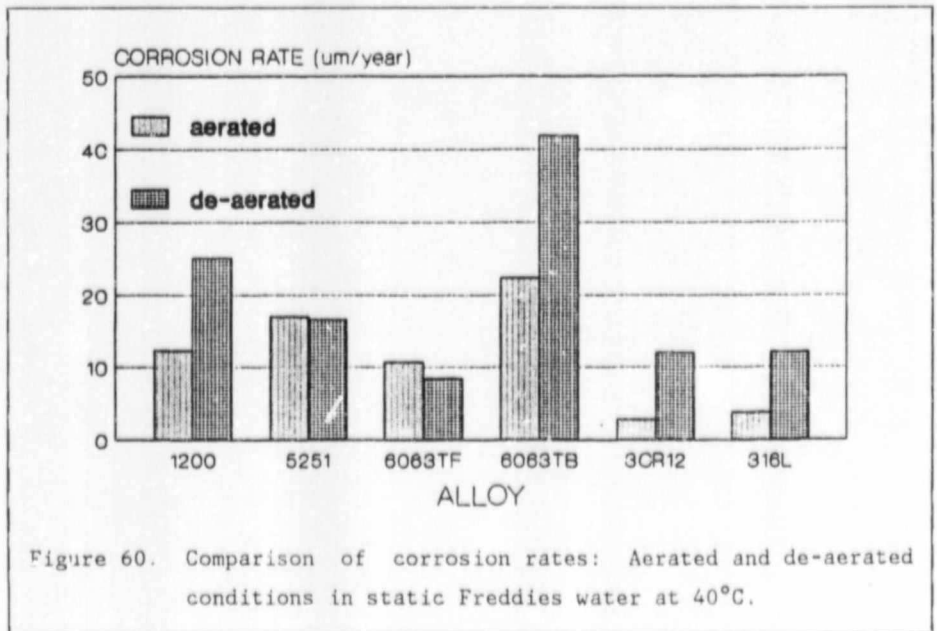
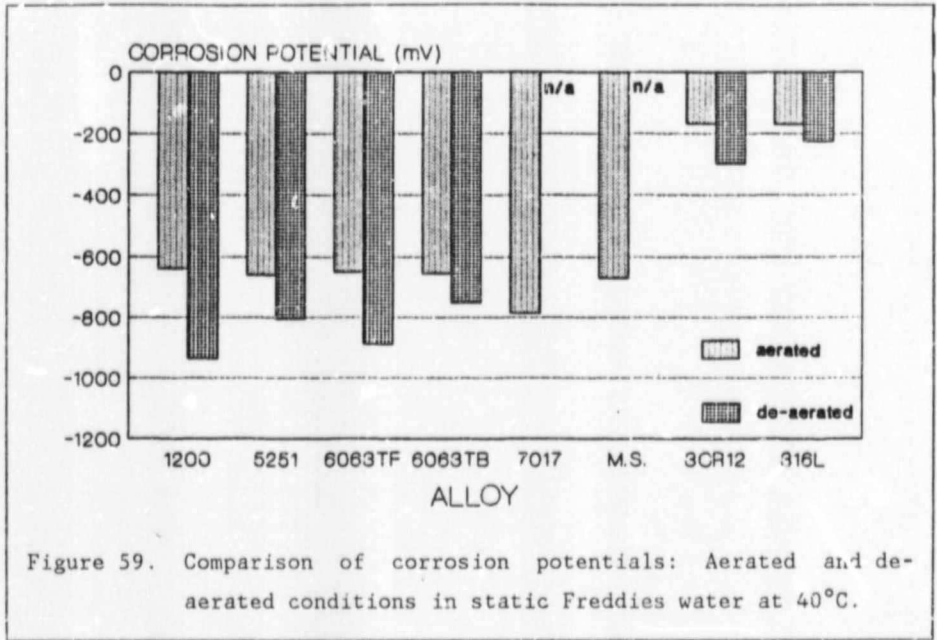
6.2.3.2 De-aerated conditions

De-aeration appeared to have two separate effects. Firstly it had a strong effect on the free corrosion potentials and depressed them considerably. For example, E_{corr} for alloy 1200 went from -639mV in aerated conditions, to -937mV in de-aerated conditions. The second effect was the increase in the corrosion rate. This can be expected with active/passive metals as without oxygen present the passive film will not be able to repair itself where it has broken down. Table 6.13 contains the E_{corr} and corrosion rate values.

Table 6.13 E_{corr} and corrosion rate values for Freddie's Mine Water at 40°C under de-aerated conditions.

Alloy	Average Corrosion Potential (mV)	Average Corrosion Rate ($\mu\text{m}/\text{year}$)
1200	-937	25,1
3004	-896	-
5251	-804	16,6
6063TB	-860	41,9
6063TF	-840	18,5
3CR12	-299	12,0
316L	-266	12,1

Figures 59 and 60 show comparisons of the E_{corr} and corrosion rate values under aerated and de-aerated conditions.



6.2.4 CYCLIC POLARISATION SCANS IN FREDDIES WATER, STATIC CONDITIONS.

This section includes only the tests performed at 40°C.

6.2.4.1 Aerated water

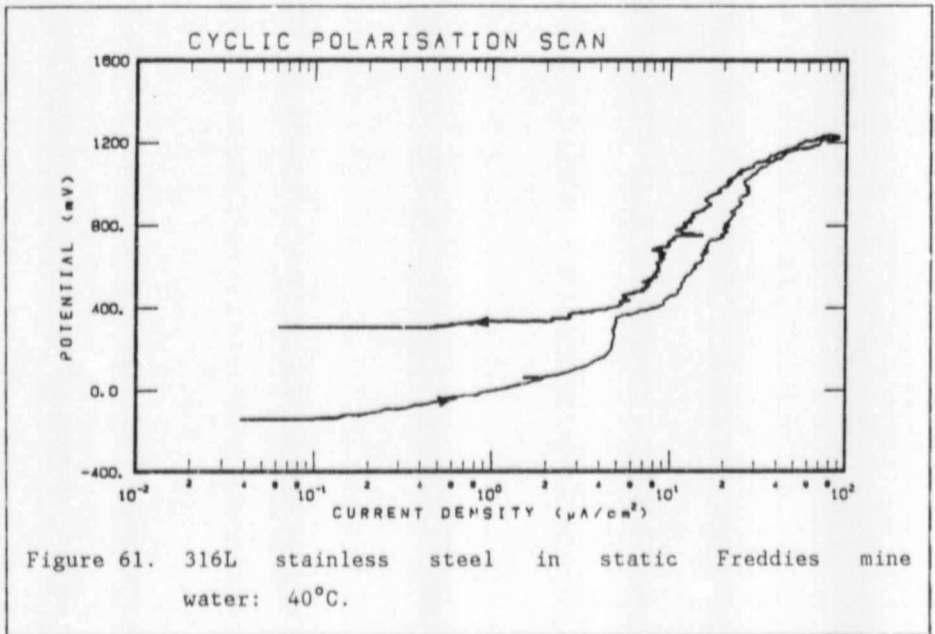
The results are summarised in Table 6.14.

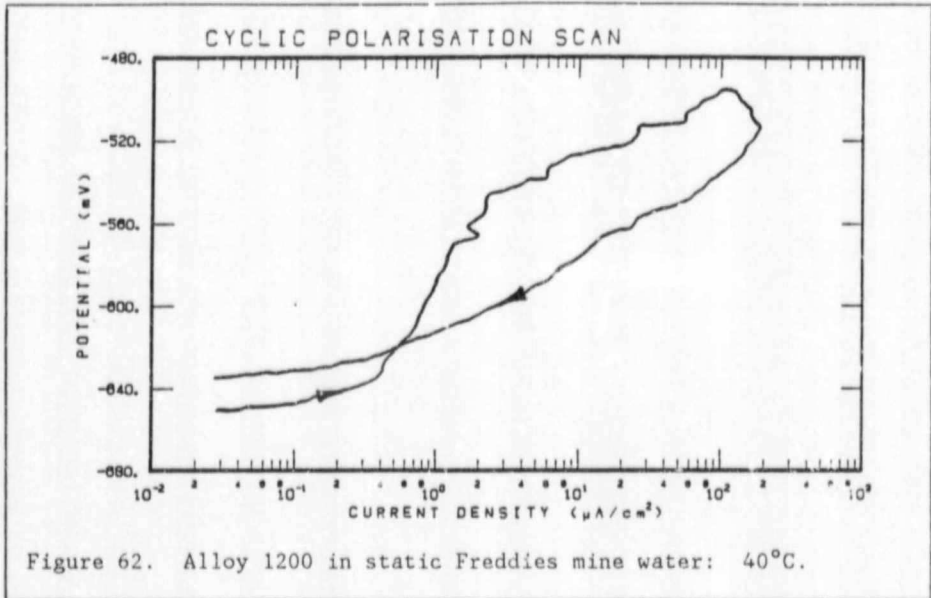
Table 6.14 Data from cyclic polarisation scans in static, aerated Freddie's water at 40°C.

Alloy	Corrosion Potential (mV)	Pitting Potential (mV)	Passive Range (mV)	Perfectly Passive Range (mV)
1200	-639	-551	88	30
3004	-623	-562	61	30
5251	-659	-552	107	0
6063TB	-649	-532	117	0
6063TF	-654	-522	132	0
3CR12	-168	+133	301	176
316L	-169	+1066	1235	1235

From these data it can be seen that only alloys 1200 and 3004 have a region of perfect passivation, but it is so limited that any minor change in the system could cause it to disappear. The passive ranges are all very small, being only of the order of 100mV. 3CR12 does have a perfectly passive range, but at 176mV this can be considered to be too small for the safe use of this alloy. 316L stainless steel is fully passive with both the

passive and perfectly passive ranges being the same. Thus there is no hysteresis loop, an indication of satisfactory crevice corrosion resistance. Alloys 1200 and 3004 had large hysteresis loops, as did 3CR12 and so poor crevice corrosion behaviour can be expected from them. Figure 61 illustrates the pitting behaviour of 316L stainless steel, while Figure 62 shows that of alloy 1200.





6.2.4.2 De-aerated water

De-aeration again has had a major effect on the behaviour of the alloys in that it has made the free corrosion potential more negative, and has increased the size of the passive regions.

Table 6.15 Data from cyclic polarisation scans in static, de-aerated Freddie's Mine Water at 40°C.

Alloy	Corrosion Potential (mV)	Pitting Potential (mV)	Passive Range (mV)	Perfectly Passive Range (mV)
1200	-937	-531	406	432
3004	-896	-517	379	313
5251	-904	-540	364	161
6063TB	-890	-467	423	0
6063TF	-751	-633	118	0
3CR12	-299	+50	349	95
316L	-226	+1013	1239	1239

What is most interesting here is that the increase in the passive range has come from E_{corr} decreasing, while E_p has remained essentially the same.

6.2.5 TOTAL IMMERSION TESTS - FLOW CONDITIONS.

On removal from the flow loop, the specimens all showed localised mounds of corrosion product on the surface, which dried to a white colour, interspersed with a dark brown flat corrosion product. The Alclad specimens had a very rough surface consisting solely of this white corrosion product. Alloy 5251 showed far less evidence of corrosion than any of the other alloys. Figures 63, 64 and 65 show the top surface of the Alclad, 5251 and 6063TB specimens. The blue marks are the masking compound applied to the edges to try and prevent edge attack. The specimens were still wet at this stage; hence the yellow appearance of the corrosion product. Figures 66 and 69 are the upper and lower surfaces respectively of the

specimens. From left to right the specimens are Alclad, 1200, 5251, 6063TB, and 6063TF and then another set in the same order. The most severe attack appears to be on the Alclad specimens although this is more general corrosion than a pitting type. Visually ranking the alloys according to the extent of the pitting from least to most the order would be; 5251, 6063TF, 6063TB and then 1200.

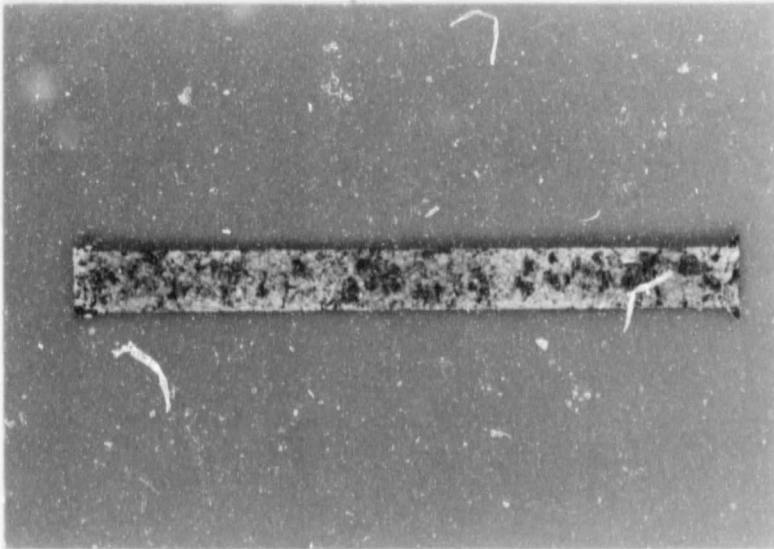


Figure 63. Upper surface of Alclad specimen after immersion in flowing water: 40°C and 1,75m/s.

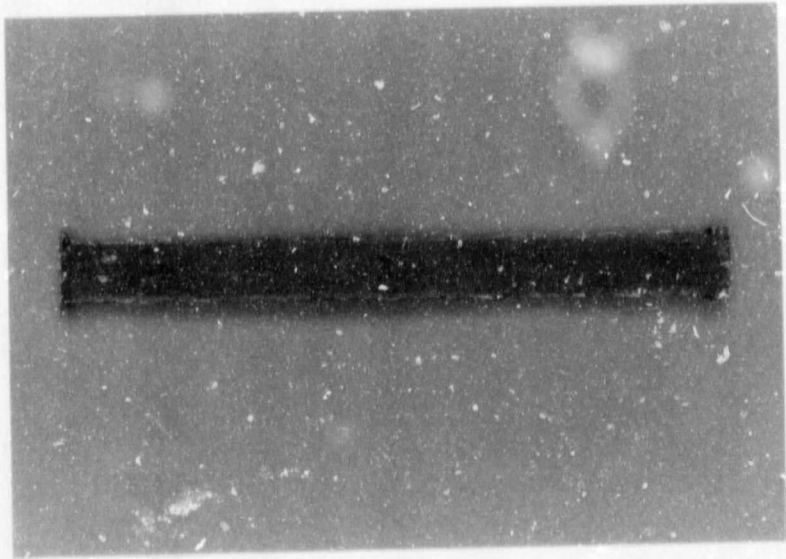


Figure 64. Upper surface of 5251 specimen after immersion: Flowing Freddies mine water at 40°C and 1,75m/s.

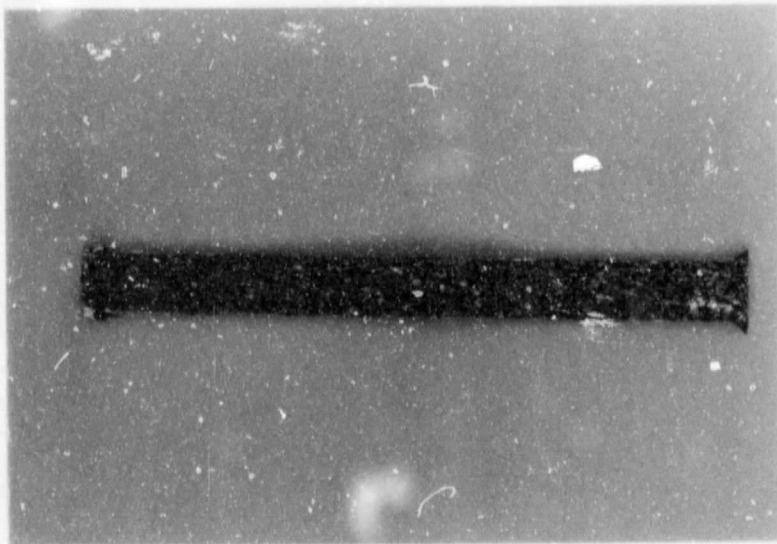


Figure 65. Upper surface of alloy 6063TB after immersion: Flowing Freddies mine water at 40°C and 1,75m/s.

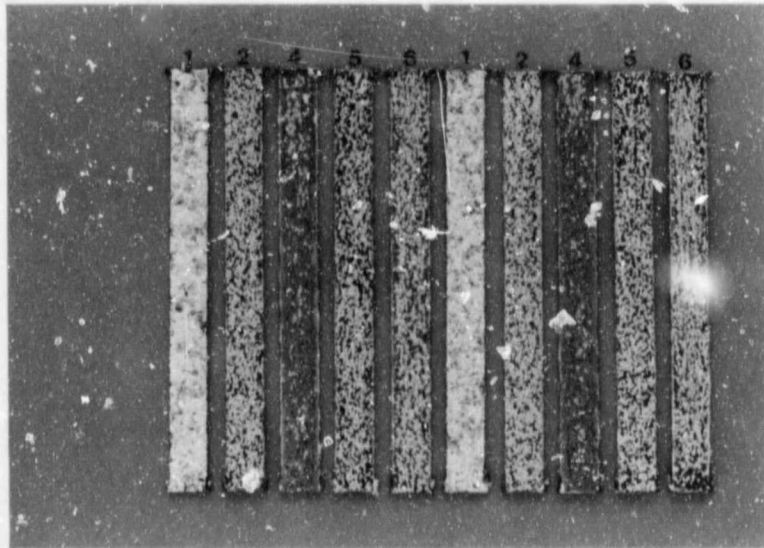


Figure 66. Upper surfaces of specimens after immersion: Flowing
Freddies water at 40°C and 1,75m/s.

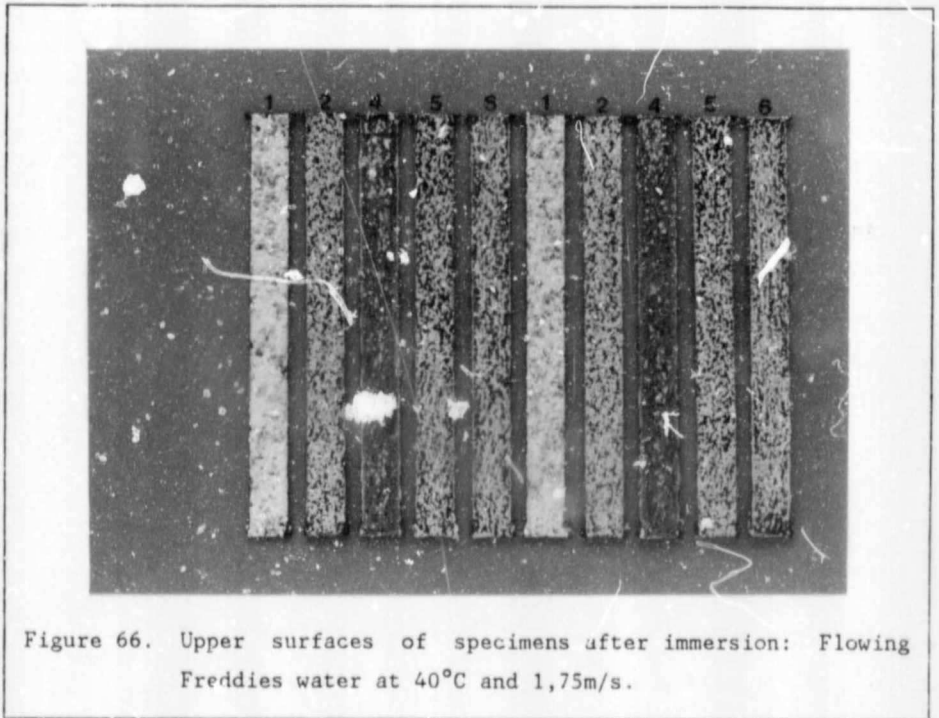


Figure 66. Upper surfaces of specimens after immersion: Flowing
Freddies water at 40°C and 1,75m/s.

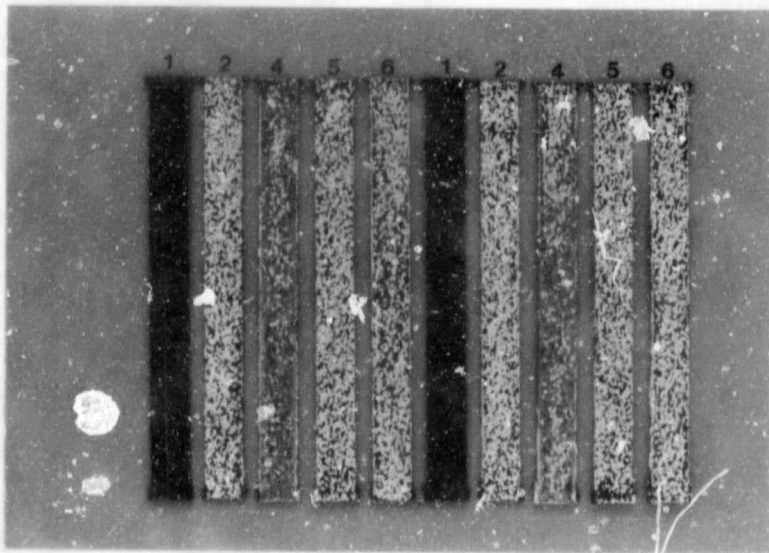


Figure 67. Lower surfaces of specimens after immersion: Flowing Freddies water at 40°C and 1,75m/s.

Examination of the specimens also revealed that the corrosion product "cap" on each pit is elongated in the direction of solution flow. (Flow direction is top to bottom in the above two photographs). It is interesting to note that there appears to be little difference in the "amount" of pitting on the upper and lower surfaces. Pitting is usually regarded as being more severe where the pits will grow downwards by gravitational effects.

After cleaning it was found that severe pitting had occurred. The Alclad specimens had very little of the original surface of the cladding left (indicated by the arrows in Figure 68). Figure 69 shows the upper surface of the first set of specimens and it can be seen that the pitting does follow the pattern that was indicated by the corrosion product on the specimens before they were cleaned.

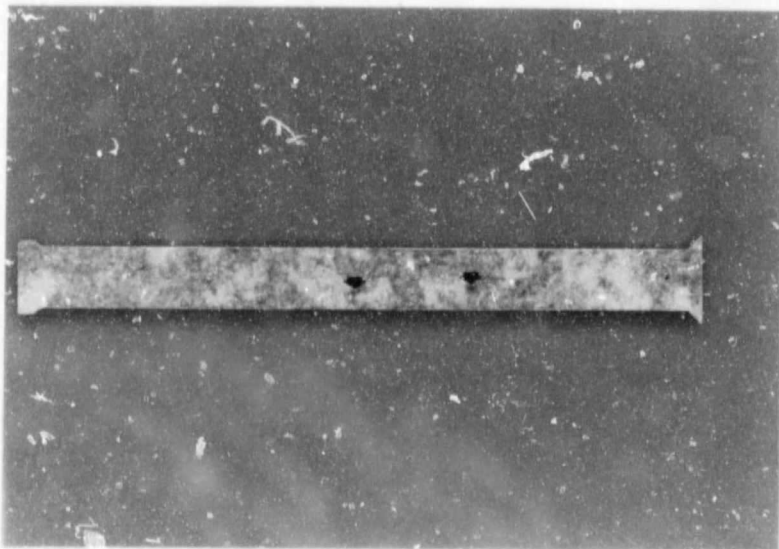


Figure 68. Cleaned Alclad specimen after immersion: In flowing
Freddies water at 40°C and 1,75m/s.

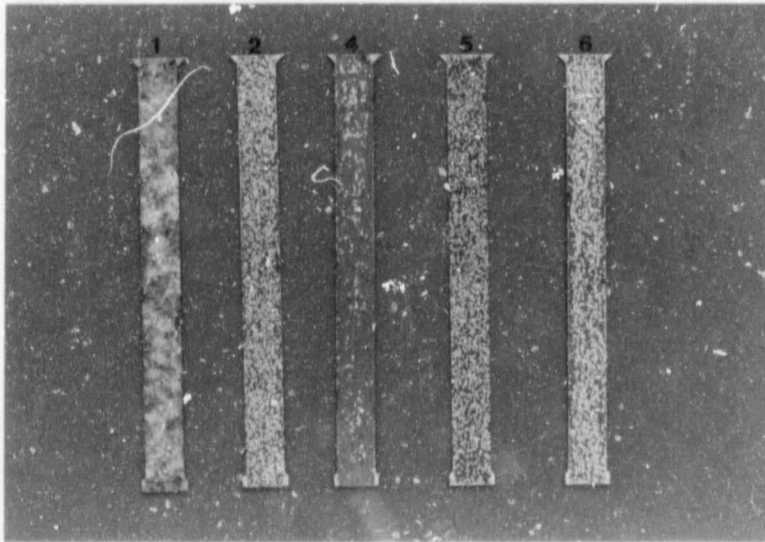


Figure 69. Upper surfaces of cleaned specimens after immersion: Flowing Freddie's water at 40°C and 1,75m/s.

Particularly interesting is that alloy 6063TB contains numerous pinhole pits as well as the much shallower and broader type (Figure 70). The other specimens had very few such pits with such a high aspect ratio.

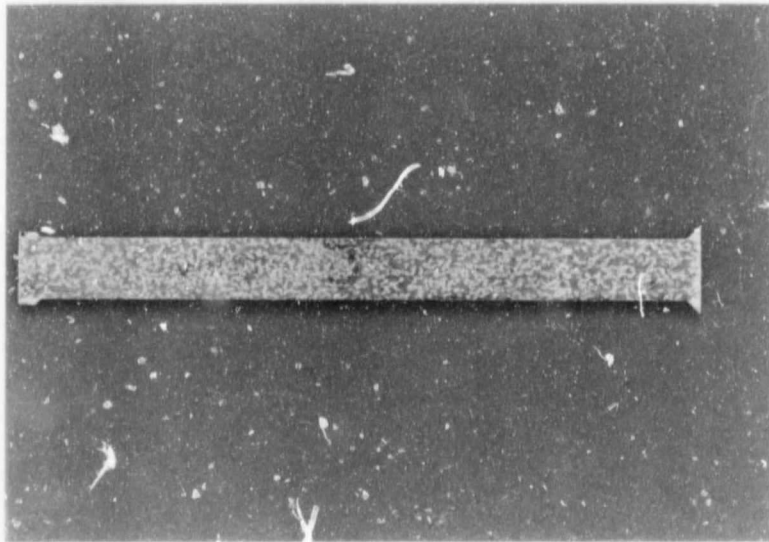


Figure 70. Cleaned surface of alloy 6063TB after immersion: Flowing Freddies water at 40°C and 1,75m/s.

6.2.5.1 Pit depths

Pit depth measurement results (Table 6.16) were interesting in that although there were far fewer pits in 5251, they were of a similar maximum depth and in fact 1200 had the shallowest pits of all the alloys tested. The Alclad specimens had no measurable pits in the base material. The cladding layer had cathodically protected the underlying metal.

Table 6.16 Pit depths in specimens exposed under flow conditions at 40°C in Freddie's Mine Water.

Alloy	Average Pit Depth (mm)	Maximum Pit Depth (mm)	Maximum Pitting Rate (mm/year)**
Alclad 1200	0,14*	0,14	-
5251	0,2	0,46	3,99
6063TB	0,14	0,71	6,15
6063TF	0,28	0,76	6,59
	0,18	0,67	5,81

Pit growth rates usually are highest initially and appear to be linear for a period that may be as long as a year as seen in various atmospheric exposure tests. After the initial period, the pit growth rate then tends to follow a relationship of the form:-

$$D = k t^{1/3} \quad (D=\text{depth, } k=\text{constant, } t=\text{time})$$

Thus the growth rate then decreases with time. However these extrapolated pit depths are very similar to results obtained by McEwan (42) over a seventeen week period in a similar water.

* - full depth of cladding layer removed, ** - assuming a linear pit growth rate

6.2.5.2 Corrosion rate results

These were calculated in units of micrometres per year ($\mu\text{m}/\text{yr}$) from the mass losses obtained for each of the specimens. These results are shown below.

Table 6.17 Corrosion rates for immersion coupons in flowing Freddie Mine Water at 40°C.

Alloy	Corrosion Rate ($\mu\text{m}/\text{yr}$)
Alclad	1151*
1200	404,9
5251	204,1
6063TE	506,2
6063TF	369,5

As expected from the visual examination, alloy 1200 had the lowest corrosion rate. The high corrosion rate of the Alclad specimen can be attributed to what is effectively galvanic corrosion once the underlying layer has been exposed. The rate can be expected to change once all of the cladding has been removed. These corrosion rates are of far less importance than the pit depths, as failure of these materials is likely to be by perforation, **not** general thinning.

* - this is really galvanic corrosion

6.2.6 TOTAL IMMERSION TESTS - STATIC CONDITIONS.

There was a marked improvement in corrosion behaviour under static conditions. There were far fewer and much shallower pits than under flow conditions.

On removal from the immersion tanks the specimens were covered with a lightly adherent, powdery, white corrosion product mainly at the edges, and a light brown/grey adherent corrosion product over the rest of the specimen (Figure 71). This white corrosion product was found at positions where the masking lacquer had partially lifted resulting in the formation of crevices. The Alclad specimens had corroded over larger areas progressing mainly from the edges. Figure 72 shows one set of these specimens, left to right in the following order; Alclad, 1200, 3004, 5251, 6063TB, 6063TF and 7017. Alloy 7017 shows general corrosion/exfoliation over most of its area and one portion where very severe corrosion has occurred. Other specimens of this material also showed similar, though not as severe localised areas of attack.

6.2.6 TOTAL IMMERSION TESTS - STATIC CONDITIONS.

There was a marked improvement in corrosion behaviour under static conditions. There were far fewer and much shallower pits than under flow conditions.

On removal from the immersion tanks the specimens were covered with a lightly adherent, powdery, white corrosion product mainly at the edges, and a light brown/grey adherent corrosion product over the rest of the specimen (Figure 71). This white corrosion product was found at positions where the masking lacquer had partially lifted resulting in the formation of crevices. The Alclad specimens had corroded over larger areas progressing mainly from the edges. Figure 72 shows one set of these specimens, left to right in the following order; Alclad, 1200, 3004, 5251, 6063TB, 6063TF and 7017. Alloy 7017 shows general corrosion/exfoliation over most of its area and one portion where very severe corrosion has occurred. Other specimens of this material also showed similar, though not as severe localised areas of attack.

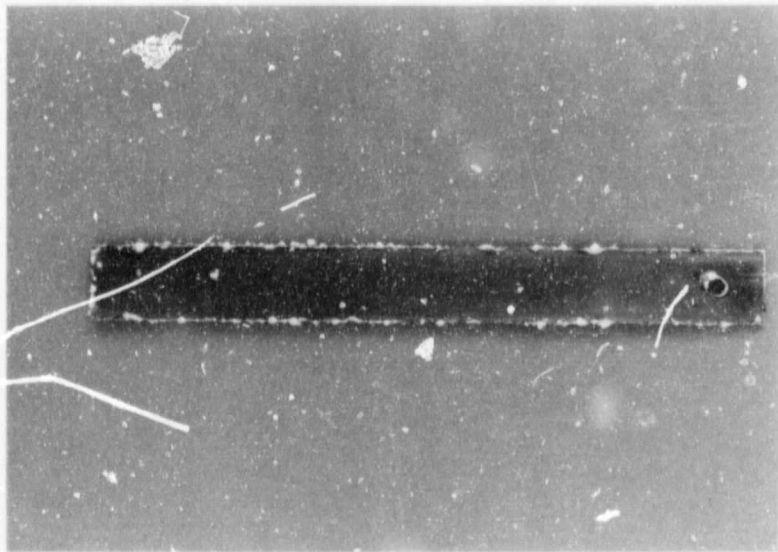


Figure 71. Alloy 1200 after immersion in static Freddies water: 40°C.

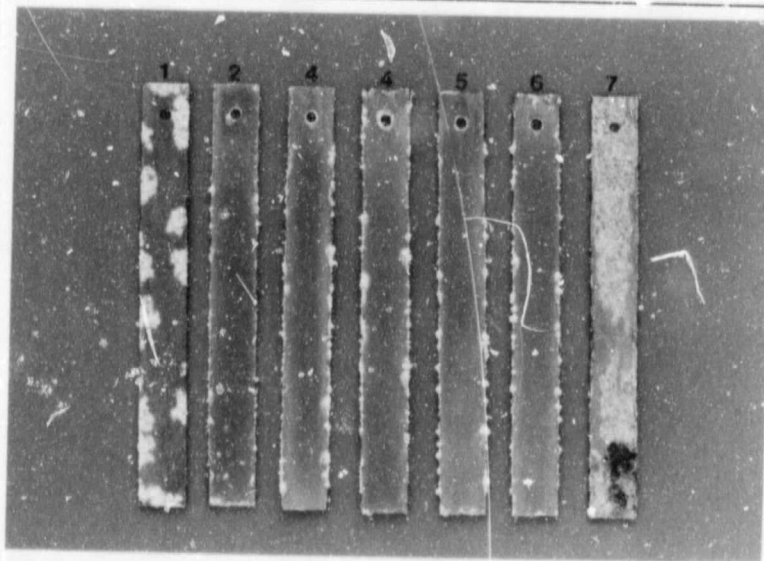


Figure 72. Specimens after immersion in static Freddies water: 40°C.

After being cleaned (Figure 73) it can clearly be seen that most of the corrosion has initiated from the edges of the specimens. Pits had formed in some of the Alclad specimens also at positions away from the edges.

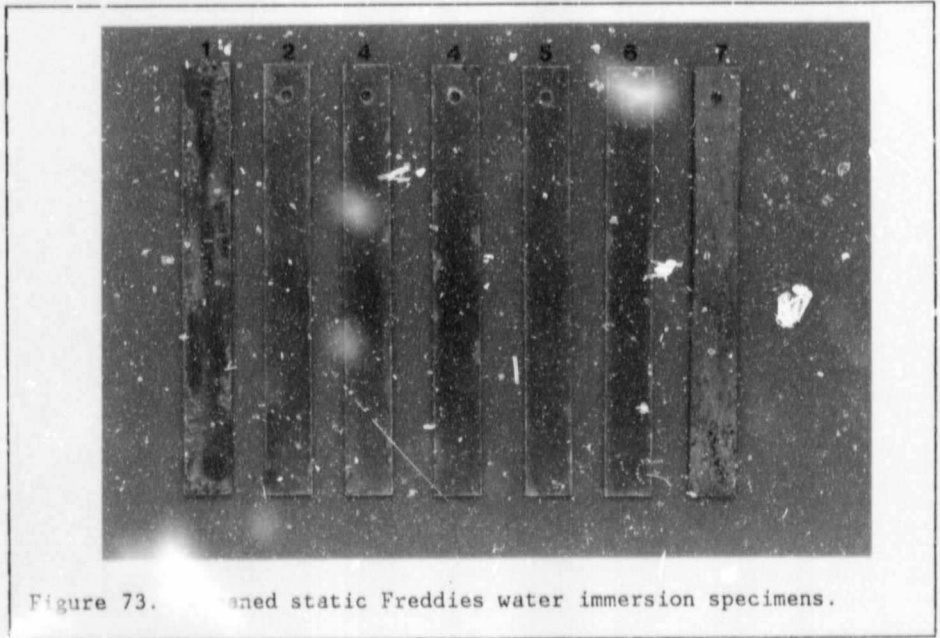


Figure 73. Corroded static Freddie's water immersion specimens.

6.2.6.1 Pit depths.

These were considerably less than under flow conditions.

Table 6.18 Pit depths in specimens exposed at 40°C in static Freddie's Mine Water.

Alloy	Average Pit Depth (mm)	Maximum Pit Depth (mm)	Maximum Pitting Rate (mm/yr)
Alclad	0,14	0,14*	-
1200	0	0***	-
5251	0	0	-
6063TB	-	0,22	1,91
6063TF	0,15	0,22	1,91
7017	0,88	1,74***	15,08

Pitting was too low to be measurable (<0,01mm) on alloys 1200 and 5251. Alloy 6063TF had the most pits. The huge pitted/exfoliated area on one of the 7017 specimens is reflected in the above table of results. However the majority of the specimen had undergone general corrosion.

6.2.6.2 Corrosion rates

The corrosion rates obtained were much lower than under flow conditions. The following table summarises these results.

* - full depth of cladding, ** - for values of 0 there were either no pits visible macroscopically, or they were less than 0,01mm deep, *** - mainly general corrosion with a few pits.

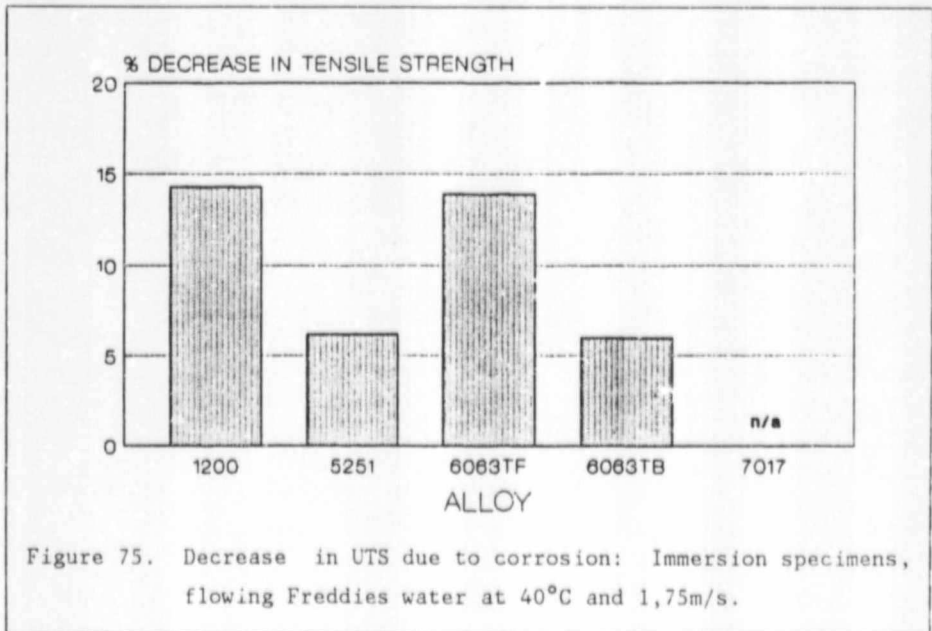
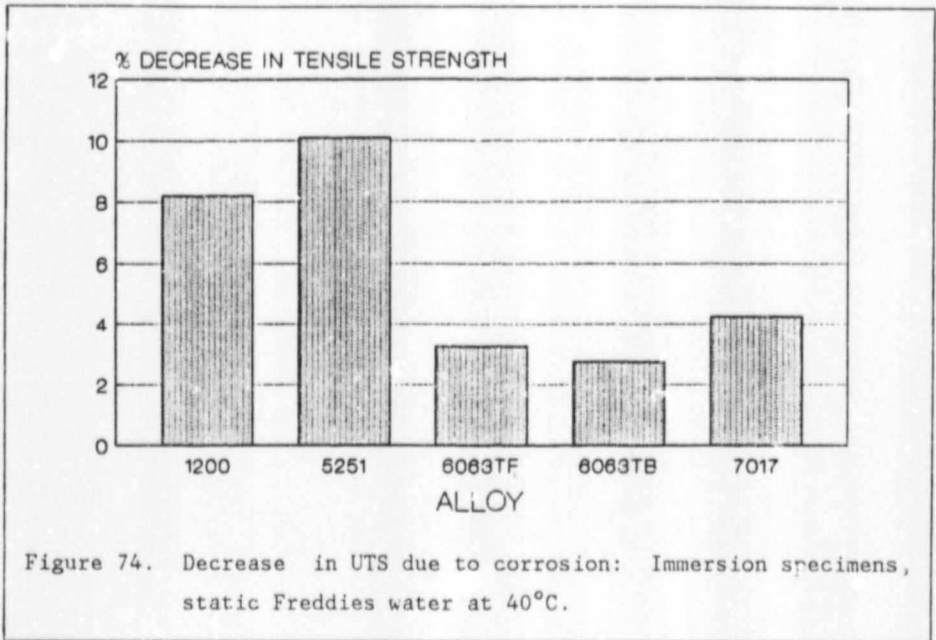
Table 6.19 Corrosion rates obtained from immersion specimens in static Freddie's Mine Water at 40°C.

Alloy	Corrosion Rate ($\mu\text{m}/\text{yr}$)
Alclad	159
1200	42,6
5251	59,1
6063TB	46,1
6063TF	45,2
7017	181,2

There is really little difference in the performance of alloys 1200 to 6063TF. It is interesting to note that 5251 had the highest corrosion rate of these 5 alloys instead of the least as under flow conditions. As expected 7017 corroded at a very high corrosion rate.

6.2.7 TENSILE TESTS

The percentage change in the ultimate tensile strength (UTS) of each alloy was determined after corrosion testing. All the Alclad specimens had a **gain** in tensile strength. There are two probable causes for this. The first is that the low strength cladding yields first and this is where the failure begins and so with this layer removed the initiation of failure is delayed. The second is that the increases are less than 5% which is within possible experimental error. The average decrease in UTS is shown in Figures 74 and 75.



As only 2 to 3 test specimens were available the results are highly dependent on the location of pits on the specimens. If a pit is at the edge of a test sample, then obviously it will have a far greater effect than if it is elsewhere.

6.3 OPTICAL MICROSCOPY

Specimens from each of the aluminium alloys used were polished and etched for microstructural examination. This was mainly to confirm the presence of the dispersed intermetallic compounds. Metallography also provided an indication of both the size and distribution of these particles and their resultant positions relative to the corrosion and pitting processes. The cladding on the Alclad was shown to be 10% of the overall thickness i.e. 0,12mm. It could clearly be seen as it had far fewer particles than the base metal.

Alloy 1200 had scattered large particles of between 1 and 5 μ m and some smaller particles of the order of 0,1 μ m. There was no banding in either the transverse or longitudinal direction.

Alloy 5251 also had large intermetallic particles of up to 13 μ m and approximately half of these were equiaxed.

Also present were numerous fine particles 0,2 μ m in diameter. No banding was evident.

Alloys 6063TB and 6063TF were similar in microstructure with large particles of approximately 5 μ m long and small particles of 0,2 μ m. 6063TF had fewer large particles than 6063TB. In these alloys the intermetallic compounds were mostly at the grain boundaries.

Alloy 7017 had the highest visible concentration of particles (large ones up to 10 μ m) with a pronounced directional effect.

6.4 SCANNING ELECTRON MICROSCOPY

The scanning electron microscope (SEM) was used to examine the corroded surfaces, sections through the pits, and the corrosion products. The description of the corrosion products is included together with the EDAX results in the next section. This section looks at typical pit morphologies for each alloy both in plan and cross section.

6.4.1 ALCLAD

The Alclad layer tended to be so severely corroded especially under flow conditions, that pieces would become detached from the surface. Figures 76 and 77 show views of the pitted area and a section through a corroded specimen, showing severe corrosion of the cladding layer. Cracking has taken place below the surface so that large portions become detached. Where the base metal had been exposed it was free of pits due to the cathodic protection by the cladding. A scratch appeared to be the site of initiation of the small pit (10 μ m) shown in Figure 78.

6.4 SCANNING ELECTRON MICROSCOPY

The scanning electron microscope (SEM) was used to examine the corroded surfaces, sections through the pits, and the corrosion products. The description of the corrosion products is included together with the EDAX results in the next section. This section looks at typical pit morphologies for each alloy both in plan and cross section.

6.4.1 ALCLAD

The Alclad layer tended to be so severely corroded especially under flow conditions, that pieces would become detached from the surface. Figures 76 and 77 show views of the pitted area and a section through a corroded specimen, showing severe corrosion of the cladding layer. Cracking has taken place below the surface so that large portions become detached. Where the base metal had been exposed it was free of pits due to the cathodic protection by the cladding. A scratch appeared to be the site of initiation of the small pit (10 μ m) shown in Figure 78.

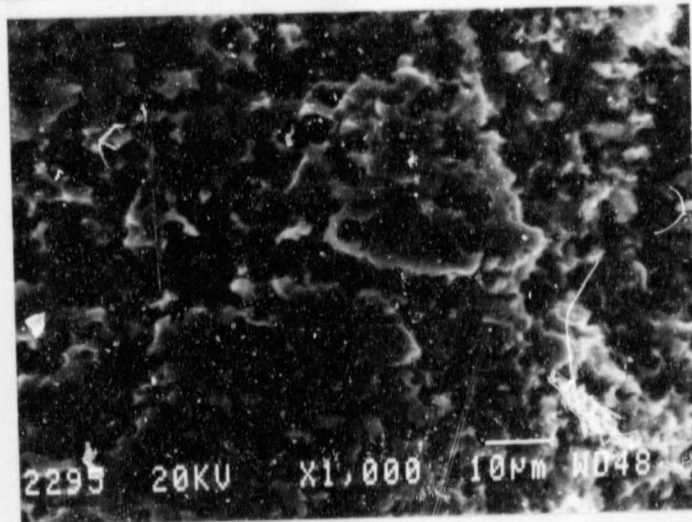


Figure 76. Pitted cladding layer on Alclad specimen: (1000x).

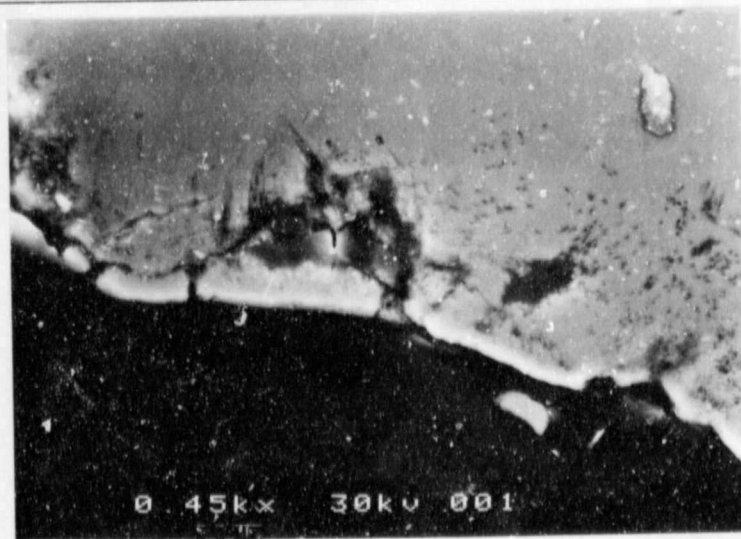


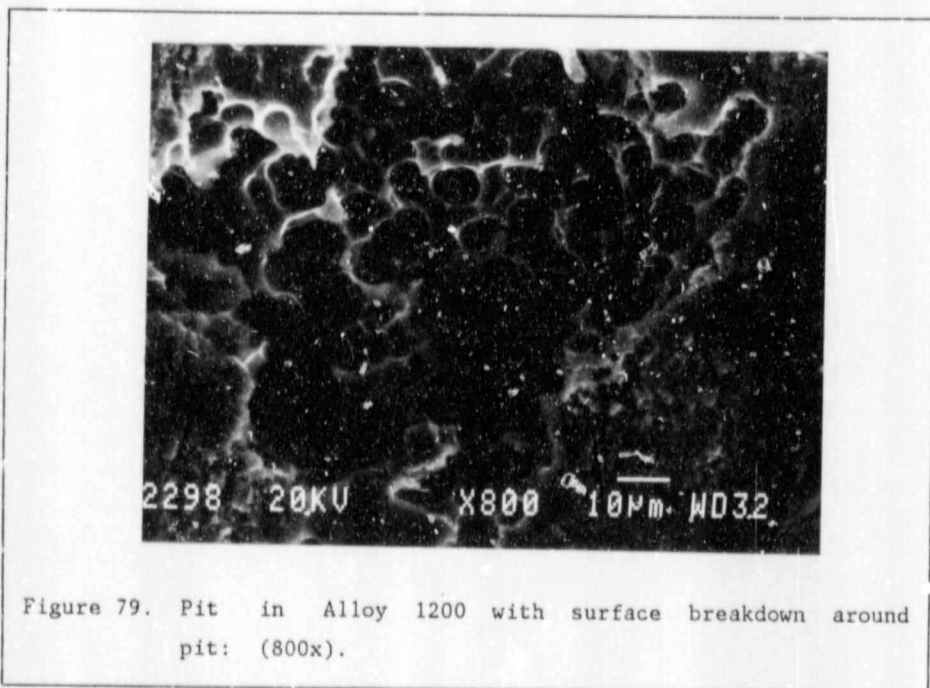
Figure 77. Cross section of specimen showing breakdown of cladding layer: (450x).



Figure 78. Pitting initiated by a surface scratch in an Alclad specimen: (2500x).

6.4.2 ALLOY 1200

Under static conditions the pits were generally of circular shape. Figure 79 shows a recently initiated pit where little penetration has occurred yet. The surface at the edges of the pit is breaking down. The cross section through a pit in this material shows the typical open, hemispherical pit that was encountered in this material. This pit is approximately 0,25mm deep.



6.4.3 ALLOY 3004

The $MnAl_6$ particles have virtually the same potential or are slightly cathodic to the aluminium (9) so that they are not preferentially corroded out. This alloy was found to have one of the highest pitting resistances measured by electrochemical tests.

6.4.4 ALLOY 5251

In Al-Mg alloys the solid solution is anodic to aluminium and its alloys. The Mg_2Al precipitates are considerably anodic to even the solid solution

and will thus undergo preferential corrosion as shown in Figure 80. The silicon tends to bring the solid solution potential closer to that of aluminium.

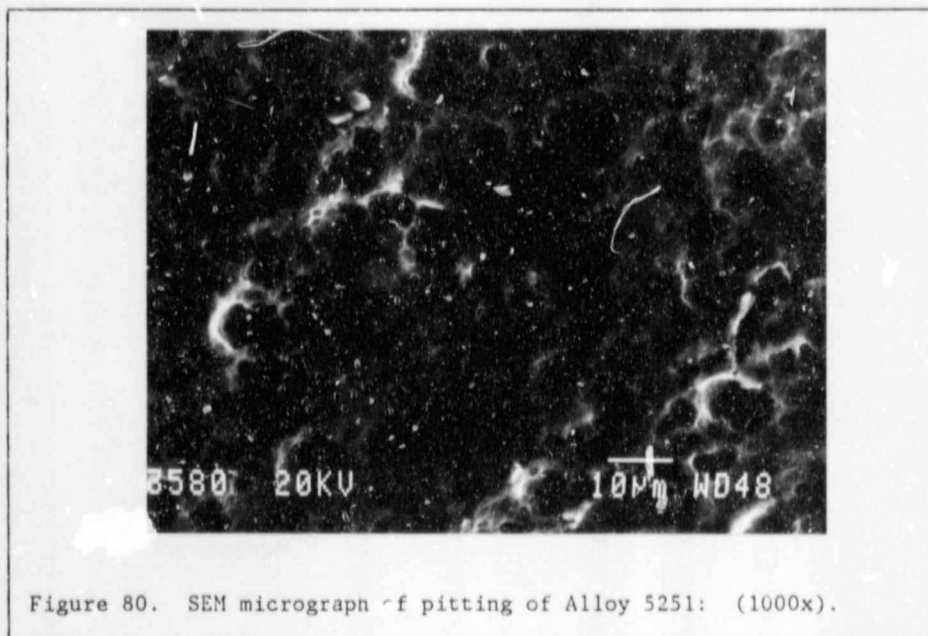


Figure 80. SEM micrograph of pitting of Alloy 5251: (1000x).

Although this alloy is known for good pitting resistance it did show severe pitting. From the surface the pits did not appear to be "large", but this alloy tended to form horizontal or semi-enclosed pits as seen in Figure 81. In Figure 82 numerous interlinked pits are shown, which together have penetrated nearly 50% through the material thickness (1,2mm thick). Some intergranular cracking along was observed due to the selective attack of precipitates at the grain boundaries.



Figure 81. Semi-enclosed pit in Alloy 5251: (550x).

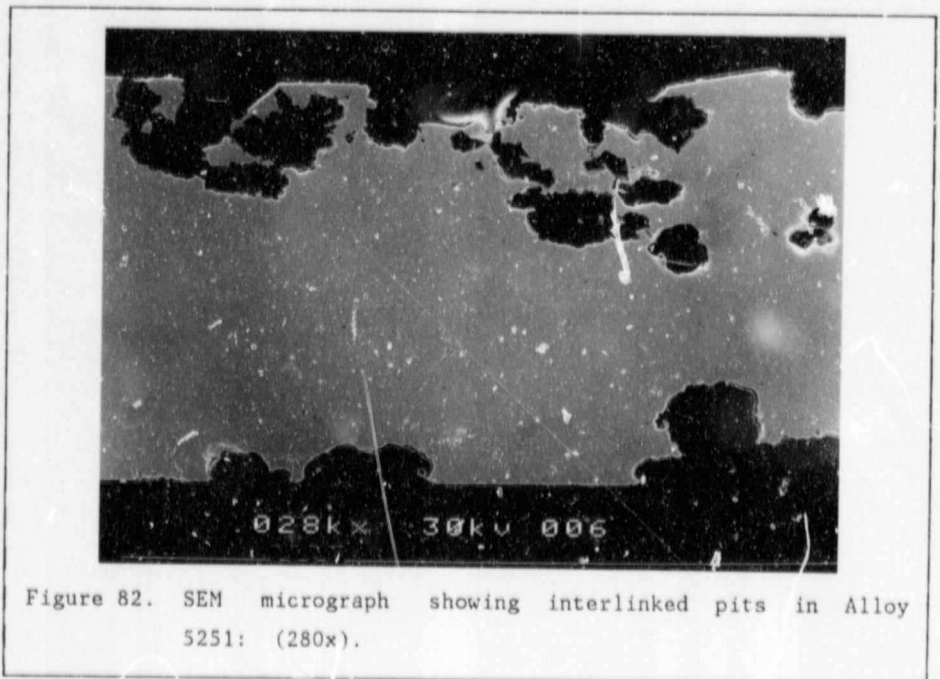
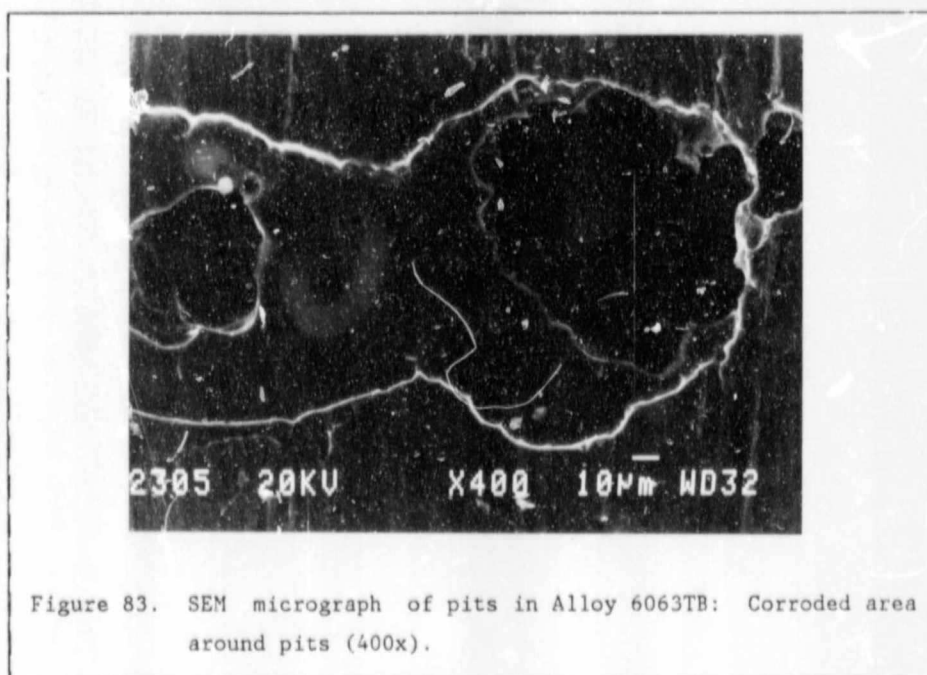


Figure 82. SEM micrograph showing interlinked pits in Alloy 5251: (280x).

6.4.5 ALLOYS 6063TB AND 6063TF

These have been grouped together, as microscopically their pitting behaviour was very similar.

Figure 83 shows pits formed under static conditions. The area covered by the corrosion product around the pit has undergone a form of crevice attack. Alloy 6063TB tended to form a more undercut type pit, while that of 6063TF was more hemispherical.



Selective corrosion of these particles at the grain boundaries took place under both static and flow test conditions. Figure 84 shows this. This pattern of attack on these two alloys could be predicted from the microstructures showing semi-continuous precipitates at the grain boundaries. Van Horn (9) gives the potential of Mg_2Al_3 as $-1,24V$ compared with that of $-0,85V$ for 99,95% Al in a 53g/l solution of NaCl.

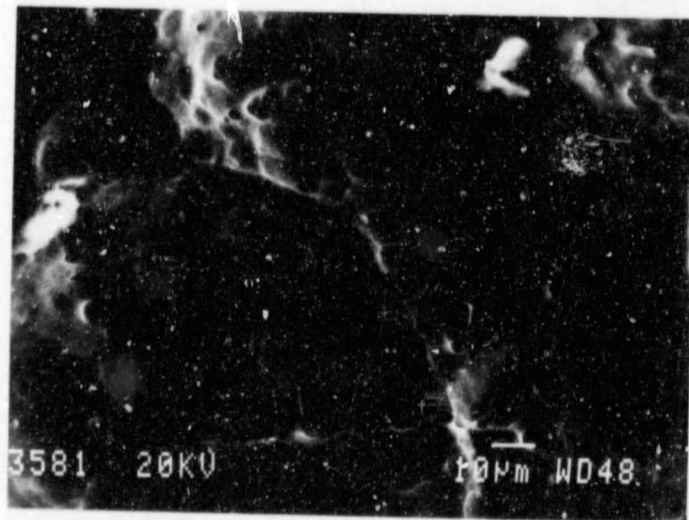


Figure 84. SEM micrograph of Alloy 6063TB: Selective attack of grain boundaries and precipitates (700x).

6.4.6 ALLOY 7017

This alloy underwent general corrosion/exfoliation attack, rather than pitting. Figure 85 shows this mode of attack with corrosion proceeding parallel to the surface before portions of the material break away. This corrosion follows the lines of banding of the particles (and the elongated grains parallel to the surface) which consist of Al+Zn and Al+Zn+Mg which are anodic to aluminium.

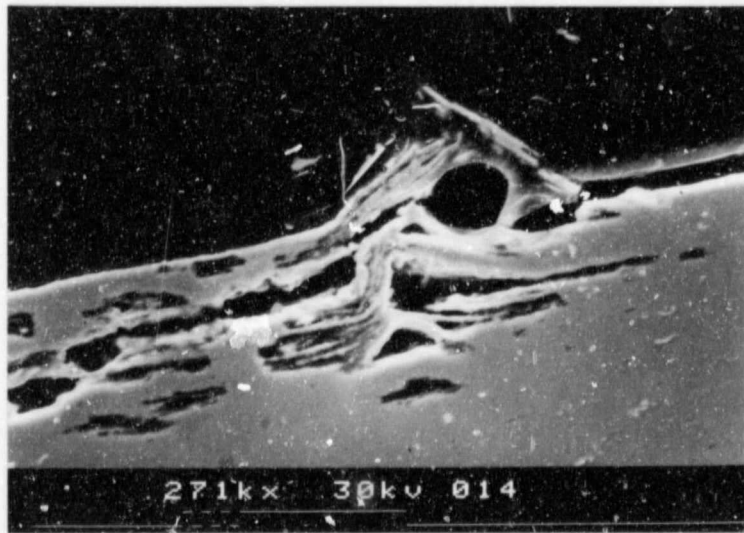
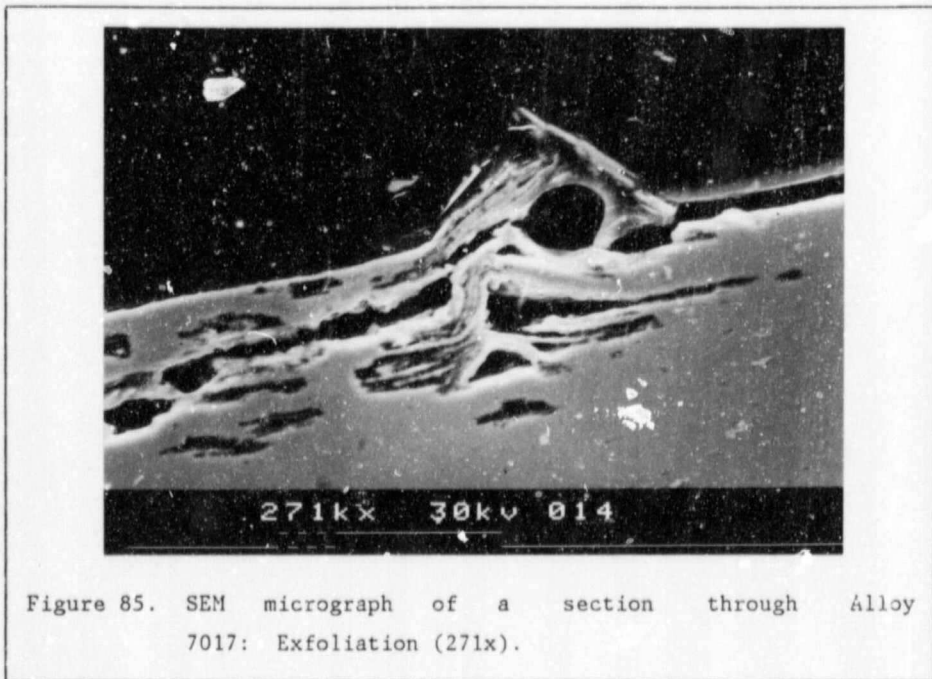


Figure 85. SEM micrograph of a section through Alloy 7017: Exfoliation (271x).

6.4.7 GENERAL COMMENTS

On all alloys there was no particular attack at the place where the specimens had been stamped with an identification number. In fact, there appeared to be less pitting there and Van Horn (9) has noted that cold working may increase resistance to corrosive attack.

It was seen especially on the flow condition specimens that pitting frequently initiated at scratches, often where two scratches intersected.



6.4.7 GENERAL COMMENTS

On all alloys there was no particular attack at the place where the specimens had been stamped with an identification number. In fact, there appeared to be less pitting there and Van Horn (9) has noted that cold working may increase resistance to corrosive attack.

It was seen especially on the flow condition specimens that pitting frequently initiated at scratches, often where two scratches intersected.

6.5 CORROSION PRODUCT ANALYSIS

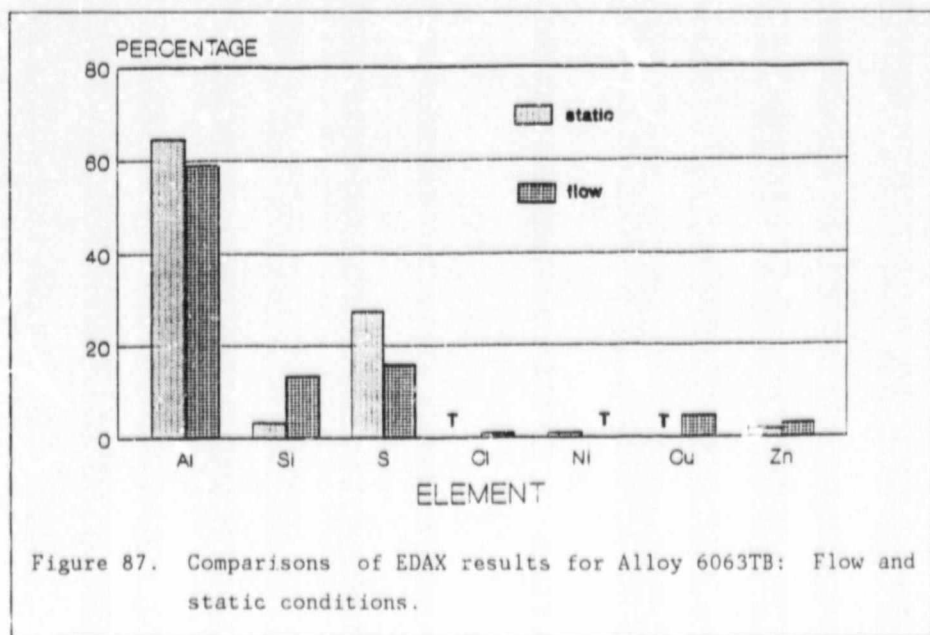
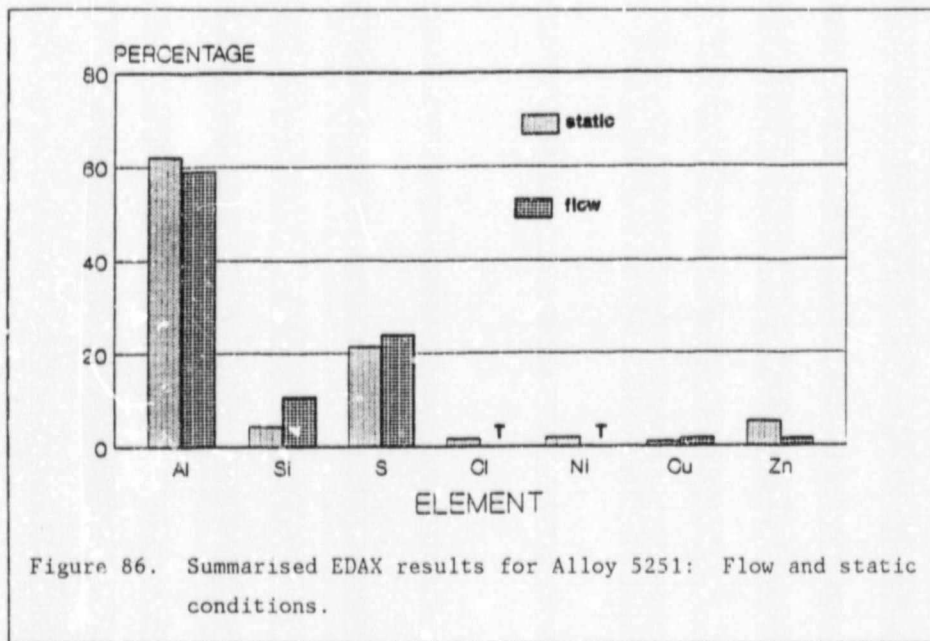
X-ray diffraction techniques could not be employed on the corrosion products which were amorphous, so that data was only obtainable from EDAX analysis. Analysis for elements from Na onwards in the periodic table was available with the particular system used. The analysis was semi-quantitative and oxygen could not be analysed for.

The main elements found were in approximate order of quantity Al>S>Si>Zn. Some of the alloys mainly the Alclad and 7017 also had Co, Ni and Cu in their corrosion products. Many of the corrosion products contained traces of Na, Cl, Ca, Mn, P, Fe and Cr.

Even though the waters contained significant levels of chlorides and it is known that they are involved in the pitting corrosion, there were only traces of Cl as the aluminium/chloride compounds (mainly $AlCl_3$) are soluble. Al/S compounds have a low solubility so they will tend to remain at the site of the corrosion. The waters used in the testing were both high in sulphates, being almost the same at 1775 and 2000ppm.

The voluminous white loosely adherent corrosion product formed on the specimens under static conditions was generally around 64% Al, 25% S and 4% Si (% by atomic weight). The more tightly adherent, darker grey or grey/brown corrosion product tended to contain less aluminium and appreciable amounts of Mn, Co, Ni, Cu, Ca, and Zn. Typical aluminium concentrations were 20-30%. The Corrosion Handbook (6) reports very similar compositions for corrosion products formed in seawater. They found the product tended to consist of amorphous $Al_2O_3 \cdot xH_2O$, Na, Cl, Cu, Mg, Mn, Zn, Ca with Ni and traces of Ti and around 16% S^{2+} and the phosphate ion.

Of considerable interest were the difference in the analysis for static and flow conditions for Freddie's Water. The bar charts shown in Figures 86 and 87 show comparisons of EDAX results produced under static and flow conditions for two alloys.



These results and others show higher levels of copper in the corrosion product under flow conditions than under static. Uhlig (45) states that traces of Cu^{2+} as low as 0,1ppm will plate out on an aluminium surface. The waters used had copper concentrations of 0,25 and 0,2ppm for Hercules and Freddie's water respectively.

The higher levels of copper in the corrosion products from flow conditions, can probably be explained by the fact that the Cu^{2+} ions have a far greater chance of coming into contact with the aluminium surface under flow conditions.

6.6 ELECTROCHEMICAL VS TOTAL IMMERSION TESTING

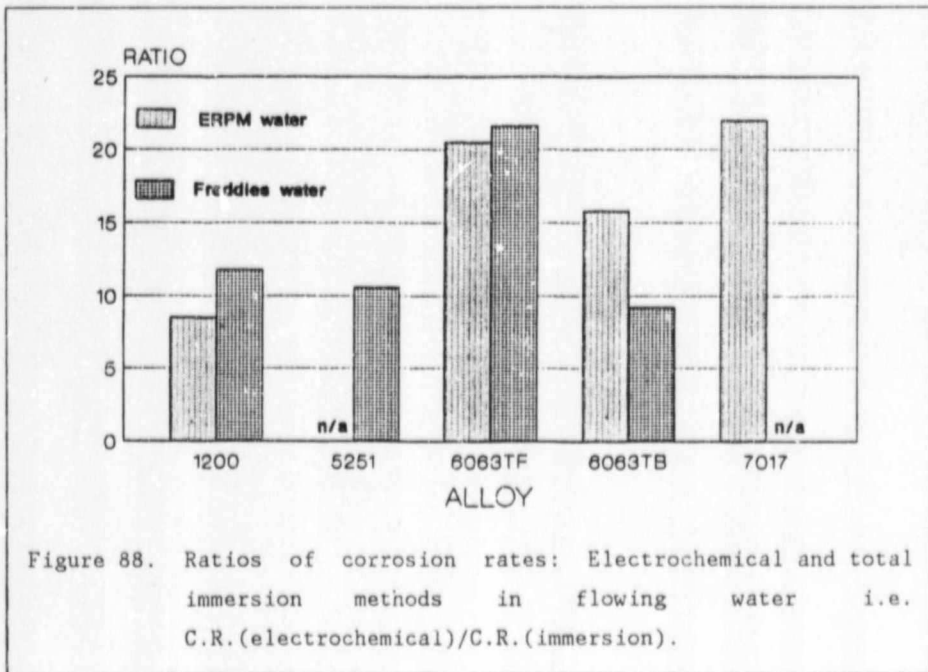
Considerable differences were found in the results obtained from the two methods. Each however, has certain advantages and disadvantages. Potentiodynamic and cyclic polarisation tests have the big advantage that they are very quick - usually only a few hours duration, while total immersion tests may take anything from weeks to years. The immersion testing however demonstrates the mode of corrosion and the geometry of pitting corrosion occurring.

Some authors have reservations about the use of corrosion rates obtained electrochemically. They place greater emphasis on the shape of the polarisation curves produced and the value of i_{corr} . However, rates produced from potentiodynamic scans are useful for comparative purposes. Errors of 100% and even 200% at low corrosion rate values are possible. Thus where the corrosion rate is critical, long term exposure of an alloy to a particular environment is necessary.

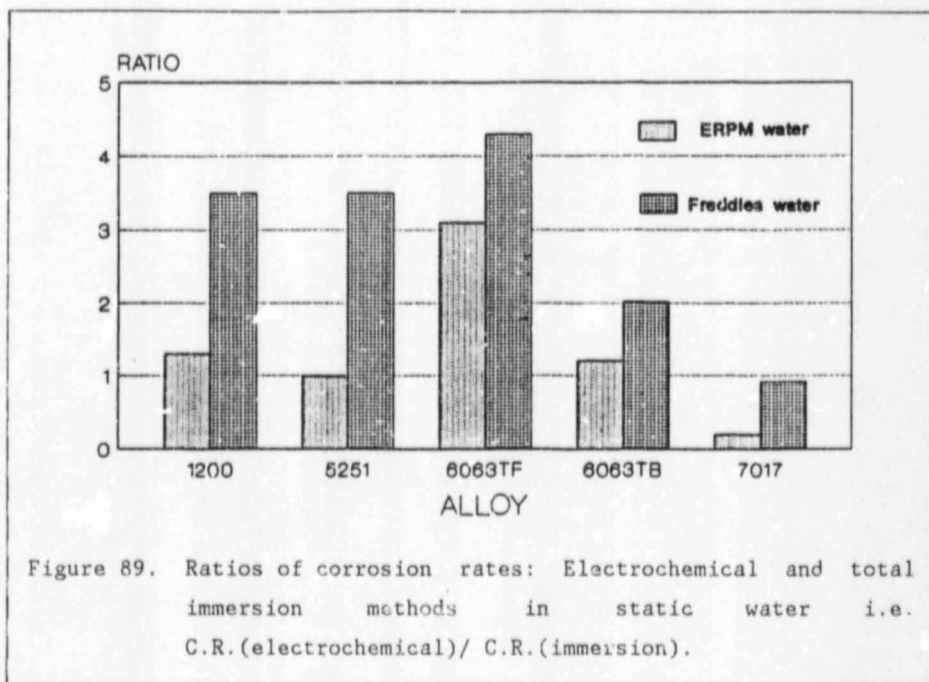
This section compares the results produced by the different methods used and produces a ranking of the materials tested in terms of their performances in mine waters.

6.6.1 CORROSION RATES FOR FLOW CONDITIONS

The ratio between the corrosion rates produced by immersion testing and those produced by electrochemical tests were calculated for each alloy and then plotted on the bar graph shown below.



The average ratios (immersion:electrochemical) for flow conditions were: 17,0:1 for Hercules Water and 13,3:1 for Freddie's water. For static conditions the ratios were much lower and these are shown in Figure 89.



Average ratio were: 1,34:1 for Hercules Shaft and 2,45:1 for Freddie's.

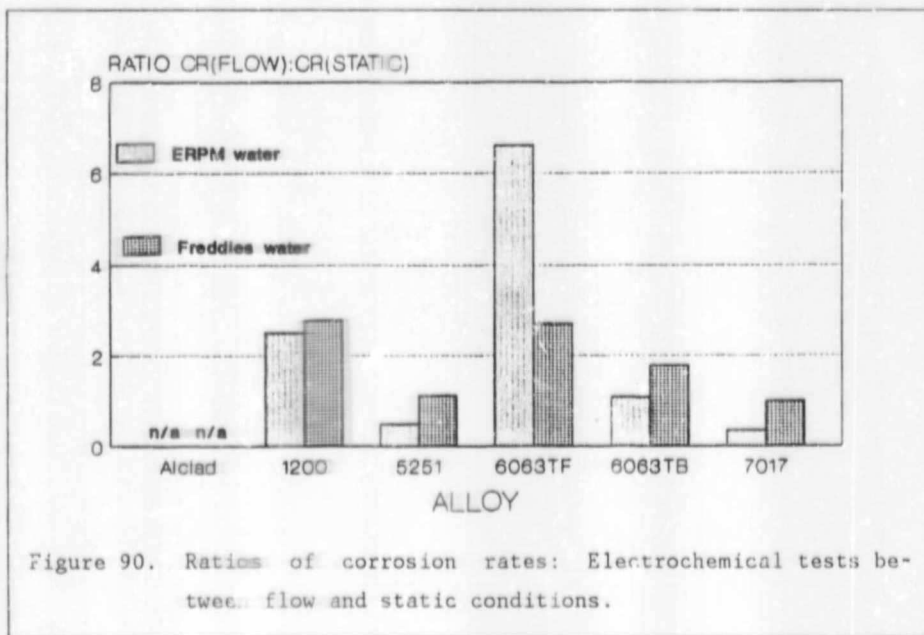
The higher ratio found under flow conditions is mainly due to the shapes of the specimens used. Since only flat specimens (i.e. sheet material) were available for the testing, coupons inserted into the test rig were used. Being at the centre of flow they would experience higher flow velocities and shear stresses than at the walls of the tube. Tubular specimens of the diameter for which the corrosion behaviour is required, would probably yield the most realistic results. This is however, frequently impractical for test purposes.

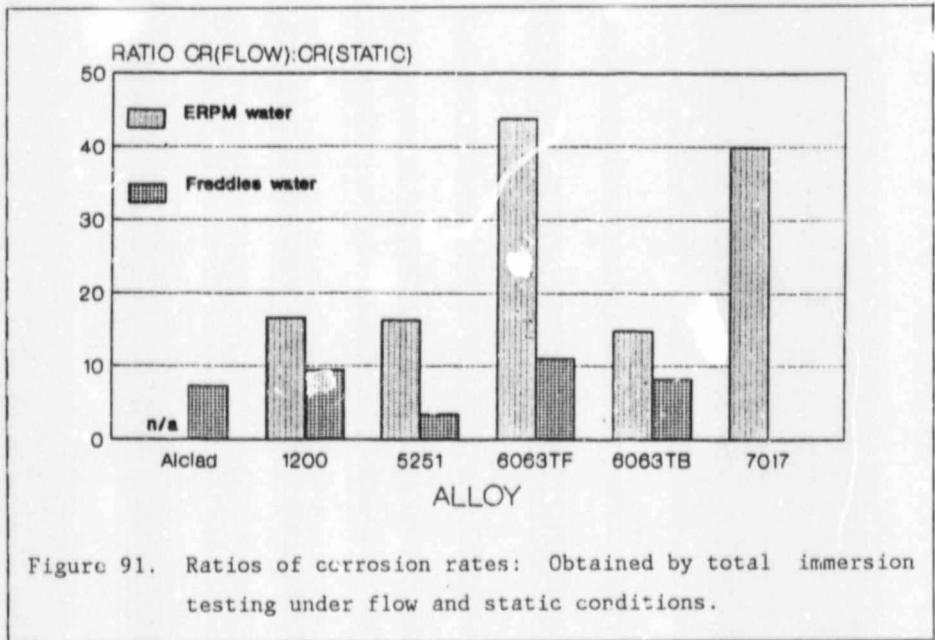
An additional reason for the difference in corrosion rates obtained by the two methods even under static conditions, is that the corrosion rate is not linear with time. Numerous studies of aluminium corrosion reported by Van Horn (9), under both atmospheric and aqueous conditions have shown that there are high initial rates which decrease greatly after approximately a years exposure.

Since the literature indicates that the initial corrosion and pitting rates tend to be the highest, the values obtained in this work can safely be assumed as being on the upper limit.

6.7 COMPARISON OF FLOW AND STATIC CONDITIONS

The data obtained from the various tests were used to draw comparisons between flow and static conditions. i.e. C.K.(Flow)/C.R.(Static). These are summarised in the following figures.





The first and obvious inference drawn from these curves is that the flow rate markedly increases the general corrosion rate. The effect also appears to vary depending both upon the alloy and the composition of the water. Alloy 6063TB for example generally appears to be affected the most by flow. It also recorded the poorest performance in terms of general corrosion and pitting in a number of the tests. This implies a less stable passive film which is thus also more likely to be effected to a greater extent by the flow water velocity.

Interestingly the corrosion rates for alloy 7017 were little influenced by water velocity in the electrochemical tests, whilst in the total immersion tests there was a marked effect. As previously discussed the mode of corrosion for this alloy in these waters was by exfoliation. In the short term tests (electrochemical), there is no time for bulk metal loss by this process. In the longer term tests, severe breakup of the surface occurred. This would be aided by water velocity, both in that increased mass transport of oxygen to the corroding surface would occur and also the mechanical action of the water would loosen surface debris. The increase in mass transport to the corroding surface becomes more im-

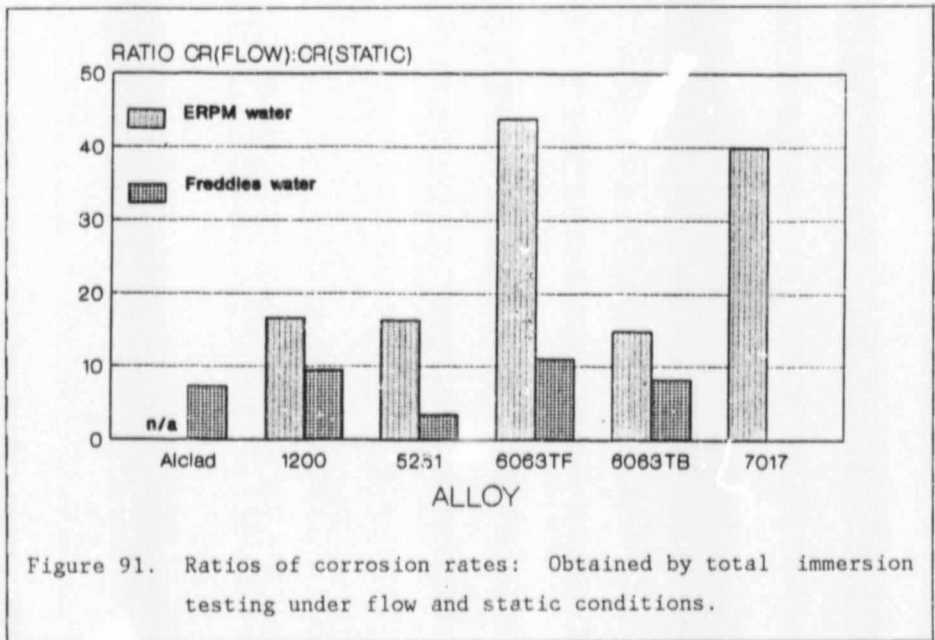


Figure 91. Ratios of corrosion rates: Obtained by total immersion testing under flow and static conditions.

The first and obvious inference drawn from these curves is that the flow rate markedly increases the general corrosion rate. The effect also appears to vary depending both upon the alloy and the composition of the water. Alloy 6063TB for example generally appears to be affected the most by flow. It also recorded the poorest performance in terms of general corrosion and pitting in a number of the tests. This implies a less stable passive film which is thus also more likely to be effected to a greater extent by the flow water velocity.

Interestingly the corrosion rates for alloy 7017 were little influenced by water velocity in the electrochemical tests, whilst in the total immersion tests there was a marked effect. As previously discussed the mode of corrosion for this alloy in these waters was by exfoliation. In the short term tests (electrochemical), there is no time for bulk metal loss by this process. In the longer term tests, severe breakup of the surface occurred. This would be aided by water velocity, both in that increased mass transport of oxygen to the corroding surface would occur and also the mechanical action of the water would loosen surface debris. The increase in mass transport to the corroding surface becomes more im-

Author Buchan Andrew John

Name of thesis Corrosion Of Aluminium Alloys In Static And Recirculating Mine Waters. 1988

PUBLISHER:

University of the Witwatersrand, Johannesburg

©2013

LEGAL NOTICES:

Copyright Notice: All materials on the University of the Witwatersrand, Johannesburg Library website are protected by South African copyright law and may not be distributed, transmitted, displayed, or otherwise published in any format, without the prior written permission of the copyright owner.

Disclaimer and Terms of Use: Provided that you maintain all copyright and other notices contained therein, you may download material (one machine readable copy and one print copy per page) for your personal and/or educational non-commercial use only.

The University of the Witwatersrand, Johannesburg, is not responsible for any errors or omissions and excludes any and all liability for any errors in or omissions from the information on the Library website.